Bi3D: Stereo Depth Estimation via Binary Classifications

Abhishek Badki[1,2]   Alejandro Troccoli[1]   Kihwan Kim[1]   Jan Kautz[1]   Pradeep Sen[2]   Orazio Gallo[1]

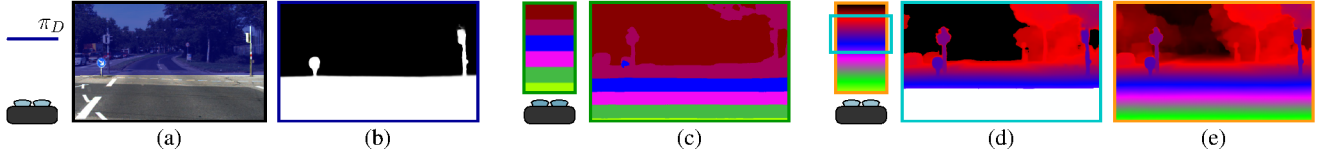[1]NVIDIA   [2]University of California, Santa Barbara

Figure 1: Our stereo algorithm, dubbed Bi3D, offers a trade off between depth accuracy and latency. Given the plane at depth D shown in the top view on the left, and overlaid on the scene in (a), our algorithm can classify objects as being closer (white) or farther (black) than D in just a few milliseconds. Bi3D can estimate depth with arbitrary quantization, and complexity linear with the number of quantization levels, (c). It can also produce continuous depth within the same computational envelope by focusing only a specific range, cyan region in the top view of (d), where pixels outside the range are still identified as closer (white) or farther (black). Finally, it can estimate the full depthmap, (e).

Abstract

Stereo-based depth estimation is a cornerstone of computer vision, with state-of-the-art methods delivering accurate results in real time. For several applications such as autonomous navigation, however, it may be useful to trade accuracy for lower latency. We present Bi3D, a method that estimates depth via a series of binary classifications. Rather than testing if objects are at *a particular depth D, as existing stereo methods do, it classifies them as being* closer *or* farther *than D. This property offers a powerful mechanism to balance accuracy and latency. Given a strict time budget, Bi3D can detect objects closer than a given distance in as little as a few milliseconds, or estimate depth with arbitrarily coarse quantization, with complexity linear with the number of quantization levels. Bi3D can also use the allotted quantization levels to get continuous depth, but in a specific depth range. For standard stereo (i.e., continuous depth on the whole range), our method is close to or on par with state-of-the-art, finely tuned stereo methods.*

1. Introduction

Stereo-based depth estimation is a core task in computer vision [21]. State-of-the-art stereo algorithms estimate depth with good accuracy, while maintaining real-time execution [4, 12].

Applications such as autonomous navigation, however, do not always require centimeter-accurate depth: detecting an obstacle within the braking distance of the ego vehicle

---

This work was done while A. Badki was interning at NVIDIA.

(with the appropriate bound on the error) can trigger the appropriate response, even if the obstacle's depth is not *exactly* known. Moreover, the required accuracy and the range of interest varies with the task. Highway driving, for instance, requires longer range but can deal with more coarsely quantized depth than parallel parking. Given a time budget for computing depth information, then, one can leverage this trade-off.

Unfortunately, existing methods do not offer the flexibility to adapt the depth quantization levels, to determine if an object is within a certain distance, or simply to focus only on a particular range of the scene, without estimating the full depth first. This is because, at their core, most existing algorithms compute depth by testing a number of candidate disparities, and selecting the most likely under some cost function. This results in two requirements on the choice of the candidate disparities for existing methods:

1. they need to span a range covering all the objects in the scene, and
2. they cannot be arbitrarily coarse.

If an object is outside the range spanned by the candidate disparities, existing methods still map it to the candidate disparity with the lower cost, as shown in Figure 8. If the disparity candidates are too coarse, *i.e.*, they are separated by too many disparity levels, the correct disparity may never be sampled, which, once again, results in the wrong depth estimation.

We present a stereo method that allows us to take advantage of the trade-off between the depth quantization and the computational budget. Our approach works by estimating the *direction* of disparity relative to a given plane π, rather than regressing the absolute disparity, as existing methods

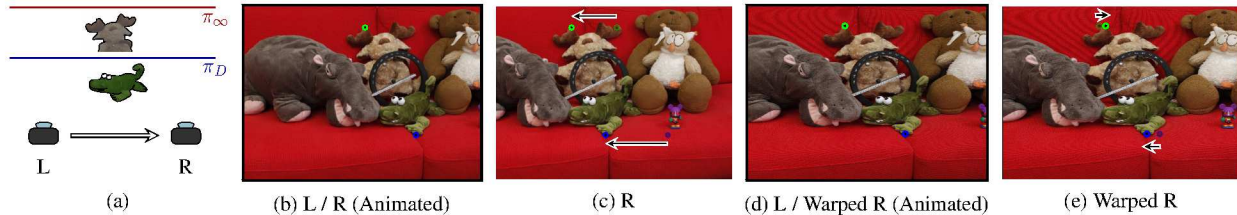| (a) | (b) L / R (Animated) | (c) R | (d) L / Warped R (Animated) | (e) Warped R |

Figure 2: Disparity, the apparent displacement of an object imaged by two cameras, is inversely proportional to the object's depth. Depth, then, can be estimated by regressing the magnitude of the disparity vectors. This is the operating principle of existing algorithms. The direction of the disparity vectors, however, is the same for all the objects in the scene. After warping both images to a plane in space π_D, the disparity of objects on opposite sides of the plane points to opposite directions. We propose to use this cue to estimate high-quality depth by classifying the direction of the disparity at multiple planes. **Figures (b) and (d) are animated. Please view in Adobe Reader and click on them to see the animation.**

do. In other words, we learn to classify points in space as "in front" or "behind" π. Plane π can be regarded as a geo-fence in front of the stereo camera that can used to detect objects closer than a safety distance. By testing multiple such planes, we can estimate the depth at which a pixel switches from being "in front" to being "behind," that is, the depth for that pixel. Note that, because our method does not need to test the plane *at or around* the actual depth of the pixel, the planes tested can be arbitrarily far from each other, allowing to control the depth's quantization. For the same reason, our method offers valuable information even for objects that are outside of the tested range—whether they are in front or beyond the range.

To illustrate the core intuition of our approach, we consider the case of a camera pair, as in Figure 2(a). Figures 2(b) and 2(c) show that the magnitude of the disparity vector carries information about depth, with larger disparities indicating objects closer to the camera. The disparity vector direction, however, does not change: all objects appear to "move" towards the left. Figures 2(c) and 2(d) show what happens when we warp the right image by the homography induced by π_D, the plane at distance D. We note that now objects appear to be "moving" in different directions: the disparity vector direction for objects at, or in front plane π_D is the same as before, while for objects beyond plane π_D it flips: it is now towards the right. We leverage this observation and classify the direction of the disparity vector, rather than to accurately regress its magnitude. If we repeat this task for several planes progressively closer to the camera, the depth of the plane at which the direction of the parallax vector associated with a 3D point flips yields the depth of the point. A disparity vector that never flips indicates a 3D point that is in front or beyond all of the tested planes—it is outside of the search range. Note, however, that the direction does tell us if the point is in front of beyond the search range, which is valuable information. Standard methods, in contrast, will generally assign each pixel a depth within the search range, even if the true depth is outside of this range.

In this paper we show that Bi3D, our stereo depth estimation framework, offers flexible control over the trade-off between latency and depth quantization:

- Bi3D can classify objects as being closer or farther than a given distance in a few milliseconds. We call this *binary depth estimation*, Figure 1(b).
- When a larger time budget is available, Bi3D can compute depth with varying quantization and execution time growing linearly with the number of levels. We refer to this as *quantized depth*, Figure 1(c).
- Alternatively, it can estimate continuous depth in a range $[\pi_{D_1}, \pi_{D_2}]$ while identifying objects outside of this range as closer or farther than the extremes of the range. We refer to this as *selective depth estimation*, Figure 1(d).
- Finally, Bi3D can estimate the full depth with quality comparable with the state-of-the-art.

2. Related Work

Stereo correspondence has been one of most researched topics in computer vision for decades. Scharstein and Szeliski present a good survey and provide a taxonomy that enables the comparison of stereo matching algorithms and their design [21]. In their work, they classify and compare stereo methods based on how they compute their matching cost, aggregate the cost over a region, and optimize for disparity. The matching cost measures the similarity of image patches. Some metrics are built on the brightness constancy assumption, *e.g.*, sum of squared differences or absolute differences [9]. Others establish similarity by comparing local descriptors [6, 26]. The matching costs can be compared locally, selecting the disparity that minimizes the cost regardless of the context; or more globally, using graph cuts [14], belief propagation [13], or semi-global matching [8].

A common limitation of most stereo algorithms is the requirement that disparities be enumerated. This enumeration could take the form of a search range over the scanline

on a pair of rectified stereo images, or the enumeration of all possible disparity matches in 3D space using a plane sweep algorithm [3]. The result of computing the matching cost over a plane sweep volume is a cost volume in which each cell in the volume has a matching cost. Cost volumes are amenable to filtering and regularization due to their discrete nature, which makes them a powerful tool for stereo matching.

The advancement of neural networks for perception tasks also resulted in a new wave of stereo matching algorithms. A deep neural network can be trained to compute the matching cost of two different patches, as done by Zbontar and LeCun [27]. Furthermore, a neural network can be trained to do disparity regression, as shown by Mayer *et al.* [16]. But deep-learning methods can do more than matching and direct disparity regression. Recent work on stereo matching trained on large datasets, such as the SceneFlow [16] and KITTI [5] datasets can compute features, their similarity cost, and can regularize the cost volume within a single end-to-end trained model. For example, GC-Net regularizes a cost volume using 3D convolutions and does disparity regression using a differentiable soft argmin operation [11]. DPSNet leverages geometric constraints by warping features into a cost volume using plane induced homographies, the same operation that is used to build plane sweep volumes [10]. Aggregation of context information is important to handle smooth regions and repeated patterns; PSMNet [1] can take advantage of larger context through spatial pyramid pooling. GANet [28] improves cost aggregation by providing semi-global and local cost aggregation layers. The downside of large architectures is their computation cost, which make the cost of these methods unsuitable for real-time performance. To overcome this, architectures like DeepPruner [4] reduce the cost of volume matching by pruning the search space with a differentiable PatchMatch layer.

To summarize, most of the existing work in stereo correspondence is based on the computation of a discrete cost volume or fixing a disparity search range. The exception is DispNet [16], but its performance in the KITTI stereo benchmark has been surpassed by others. Our key contribution is the framing of depth estimation as a collection of binary classification tasks. Each of these tasks provides useful depth information about the scene by estimating the upper or lower bound on the disparity value at each pixel. As a result, our proposed method can be more selective or adaptive according to the task and the scene. We can also do accurate disparity regression by repeating the binary classification at multiple planes.

3. Method

Given a stereo pair, R and S, we can build a plane sweep volume (PSV) by selecting a range of disparities $\{d_i\}_{i=0:N}$. Each plane of the PSV with reference to the left image can
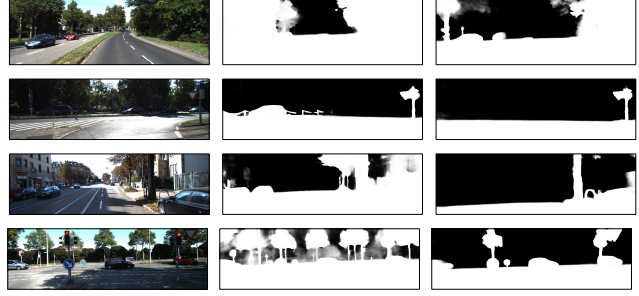

Figure 3: Given a stereo pair and π_{d_i}, the plane corresponding to disparity d_i, our method can estimate whether an object is closer or farther than π_{d_i}. For the scene shown on the left and for different depths, this results in the confidence maps shown here (white means "in front").

be computed as

$$\text{PSV}(x, y, d_i) = \mathcal{W}(S(x, y), H_{\pi_{d_i}}), \tag{1}$$

where $\mathcal{W}(\,\cdot\,, H)$ is a warping operator based on homography H, and $H_{\pi_{d_i}}$ is the homography induced by the plane at the depth corresponding to disparity d_i. (With slight abuse of notation, in the following we refer to π_{d_i} as the plane at disparity d_i.)

Given a matching cost C, then, existing algorithms find the disparity for a pixel as

$$\bar{d}(x, y) = \arg\min_{d_i} C(N_R(x, y), N_{\text{PSV}}(x, y, d_i)), \tag{2}$$

where N is a neighborhood of the pixel. The choice of the cost C varies with the algorithm. It can be a simple normalized-cross correlation of the grayscale patches centered at (x, y), or it could be the output of a neural network and, thus, computed on learned features instead [11]. Regardless of the choice,

$$\bar{d}(x, y) \in [d_0, d_N]. \tag{3}$$

Equation 3 implies that an object whose disparity is outside of the range $D = [d_0, d_N]$ is still mapped to the interval D. We argue that this a major limitation and show how it can be lifted.

3.1. Depth via Binary Classifications

Instead of estimating $\bar{d}(x, y)$ directly, we observe that the *direction* of the disparity vector itself carries valuable information. After warping image S with Equation 1, in fact, the disparity direction flips depending on whether the object is in front of π_{d_i} or behind it. The animation in Figure 2 shows the stereo pair before and after warping image S.

This suggests that we can train a binary classifier to take two images, $R(x, y)$ and $\text{PSV}(x, y, d)|_{d=d_i}$, and predict the parts of the scene that are behind (or in front of) π_{d_i}. To do this, we train a relatively standard neural network using

a binary cross-entropy loss (details on the architecture are offered in Section 4). At convergence, the classifier's output can be remapped to $[0, 1]$ producing

$$\mathcal{C}_{d_i}(x, y) = \sigma(o(x, y)), \qquad (4)$$

where o is the output of the network, and $\sigma(\cdot)$ is a sigmoid function. $\mathcal{C}_{d_i}$ can be interpreted as a measure of the classifier's confidence. When $\mathcal{C}_{d_i}$ is close to 1 or 0, the network is confident that the object is in front or behind the plane, respectively, while values close to 0.5 indicate that the network is less confident. We can then classify the pixel by thresholding $\mathcal{C}$ at 0.5. See Section 4 for more details. Figure 3 shows examples of segmentation masks that this approach produces for a few images from the KITTI dataset [5]. We refer to this operation as *binary depth* estimation. Binary depth, though based on a single disparity, already provides useful information about the scene: whether an object is within a certain distance from the camera or not—a form of geofence around the stereo camera. Existing approaches cannot infer binary depth without computing the full depth first. This is because they have to test a set of disparities to select the most likely.

We can repeat this classification for a set of disparity planes $\{d_i\}_{i=0:N}$ and concatenate the results for different disparities in a single volume $\mathcal{C}(x, y, d)|_{d=d_i} = \mathcal{C}_{d_i}(x, y)$, which we refer to as confidence volume. Figure 4(b) shows $\mathcal{C}(x, y, d)|_{(x,y)=(x_0,y_0)}$ (confidence across all the disparity planes for a particular pixel) for objects at different positions with respect to the range. Assume that an object lies within the range of disparities $[d_0, d_N]$, like object Ⓑ. For disparity planes far behind the object, the classifier is likely to be confident in predicting that the object Ⓑ is in front (*i.e.*, $\mathcal{C} = 1$). Similarly, for disparity planes much closer than the object, we expect it to be confident in predicting the opposite (*i.e.*, $\mathcal{C} = 0$). For disparity planes that are closer to the object, however, the prediction is less confident. This is understandable: the closer the plane is to the object's depth, the smaller the magnitude of the disparity vector, making the direction difficult to classify. In principle, at the correct disparity the classifier should be confused and predict 0.5. However, because of unavoidable classification noise, simply taking the first disparity at which the curve crosses 0.5 would result in large estimation errors.

To find the desired disparity, we could robustly fit a function and solve for the disparity analytically, or even train a zero-crossing network. However, we find the area under the curve (AUC) to be a simpler alternative that works well in practice:

$$\bar{d}(x, y) = \sum_{d_i} \mathcal{C}(x, y, d_i) \cdot (d_i - d_{i-1}). \qquad (5)$$

To understand the intuition behind Equation 5, consider the case in which the network is very confident for a particu-
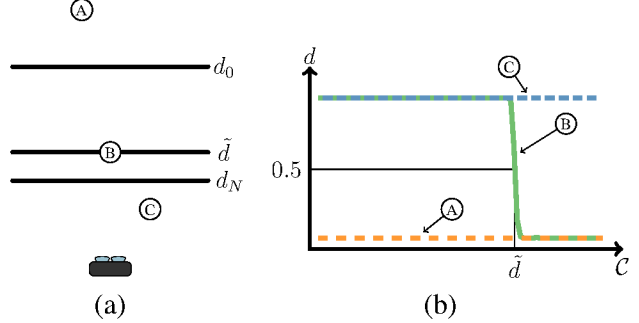

Figure 4: Actual confidence values predicted by our network for objects in different positions relative to a depth range of interest, $[d_0, d_N]$. For objects within the range, the confidence will cross the 0.5 confidence level at the object's true disparity. For objects in front or beyond the range the confidence does not cross 0.5 and stays around 1 or 0, respectively.

lar pixel (x_0, y_0):

$$\mathcal{C}(x_0, y_0, d) = \begin{cases} 1 & \text{for } d < \tilde{d} \\ 0 & \text{for } d \geq \tilde{d} \end{cases}, \qquad (6)$$

The area under the curve in Equation 5 predicts the correct value $\bar{d}(x_0, y_0) = \tilde{d}$. As shown in Figure 4, $\mathcal{C}$ is roughly linear in the region around the correct disparity. We show in the supplementary video that, under this condition, Equation 5 holds even for transitions that extend over a larger number of disparities.

Equation 5 has desirable properties. First, it exhibits some tolerance to wrong confidence values. Consider the case in which a few consecutive planes of the confidence volume of a pixel are classified confidently but incorrectly (*i.e.*, 0 instead of 1 or vice versa). An approach looking for the crossing of the 0.5 value, may interpret the transition as the desired disparity, potentially yielding a completely wrong result. The prediction in Equation 5 would just be shifted by a few disparity levels. Second, the estimate of this operation need not be one of the tested disparities: it can be a continuous value.

Figure 9 shows a comparison of the depth estimation results obtained with this method and other state-of-the-art stereo estimation approaches. Note that the visual quality of our results is on par with GwcNet [7] and GA-Net [28].

3.2. Coarsely Quantized Depth Estimation

For some use-cases binary depth may not be enough, but full, continuous depth may be unnecessary. Consider the case of highway driving, for instance: knowing that an obstacle is within, say, 1 meter of the braking distance as quickly as possible may be preferable over knowing its exact distance with a higher latency. Existing methods estimate depth by looking at all the candidate depths and use function
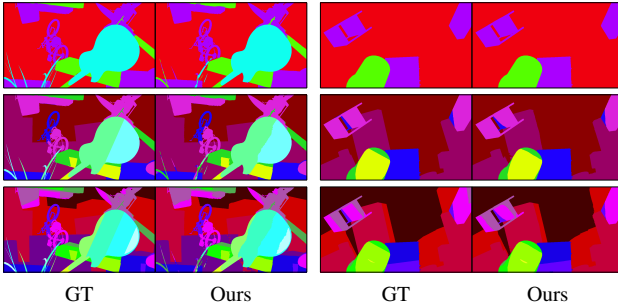
GT   Ours   GT   Ours

Figure 5: Our method can estimate depth with arbitrarily coarse quantization. Rows one through three show results for 4, 8, and 16 levels, respectively. Note that even at 4 levels one can get a basic understanding of the scene, but with much lower latency, see Table 2.

such as softargmax to achieve sub-pixel disparity. Therefore, we cannot change the coarsity at inference time or estimate depth with arbitrary quantization. Given a fronto-parallel plane π_{d_i}, which splits the range in 2 segments, Bi3D's confidence $\mathcal{C}_{d_i}(x, y)$ is related to a cumulative distribution function, CDF:

$$p(d_i \leq d(x,y)) = 1 - p(d_i > d(x,y)) = 1 - \mathcal{C}_{d_i}(x,y), \tag{7}$$

where $d(x, y)$ is the disparity of the pixel. Note that this is a proper CDF, since $\mathcal{C}_{d_i=0} = 1$ (everything is in front of the zero-disparity plane, *i.e.*, plane at infinity) and $\mathcal{C}_{d_i=\infty} = 0$ (nothing is in front of the plane at depth zero). Given a farther plane π_{d_j}, where $d_j < d_i$, then, we can write

$$p(d_j < d(x,y) \leq d_i) = \mathcal{C}_{d_j}(x,y) - \mathcal{C}_{d_i}(x,y). \tag{8}$$

Equation 8 allows to estimate depth with arbitrary quantization.

To get L quantization levels, we can use $L-1$ planes, compute the probability for each quantization bin using Equation 8 and estimate the pixel's disparity as the center of the bin (d_j, d_i) that has the highest probability. This amounts to treating quantized depth estimation as a hard-segmentation problem. If we treat it as a soft-segmentation problem, as is the case with full depth, using this CDF-based approach naturally simplifies to the AUC method described in Section 3.1.

The computational complexity is linear with the number of planes. As shown in Table 2, our method produces results that are on par with state-of-the-art methods at a fraction of the time, see Section 5.

3.3. Selective Depth Estimation

So far, we have assumed that the range $[d_0, d_N]$ covers all the disparities in the scene. Generally, this puts d_0 at 0 (plane at infinity) and d_N at the the maximum disparity expected in the scene. Since this information is not available a

priori, however, existing methods resort to using 192 disparity levels, with each disparity level being 1 pixel wide, and with $d_0 = 0$. Now consider an object outside of the range in Figure 4(a), such as Ⓒ. In this case, because they look for a minimum cost, existing methods are forced to map the object to a (wrong) depth within the range, see Figure 8. Even if they had a strategy to detect out-of-range objects, *e.g.*, threshold the cost, the best they could do would be to acknowledge that no information about the depth of the object is known.

Our strategy, on the other hand, deals with out-of-range objects seamlessly. Because the direction of the disparity vector associated with an object such as Ⓒ never changes, the confidence value $\mathcal{C}$ stays at 1 throughout the range. Therefore, in addition to knowing that Ⓒ is outside of the range we are testing, we also know that it is in front of the closest plane. If we move the farthest plane to a non-zero disparity, the same considerations apply to objects that may now be beyond the range, such as Ⓐ. Thanks to this ability, our method is robust to incorrect selections of the range.

However, we can leverage this property further. Given a budget of disparity planes that we can test, rather than distributing them uniformly over the whole range, we can allocate them to a specific range. We refer to this as *selective depth*. Selective depth allows us to get high quality, continuous depth estimation in a region of interest within the same computational envelope of quantized depth. Given a disparity range $[d_{\min}, d_{\max}]$, then, we can apply the exact same method described in Section 3.1.

Figure 8 shows selective depth results. Note that our results look like regular depthmaps that are truncated outside of the selected range. In comparison, GANet [28] struggles mapping pixels outside the range to the correct values, which affects the confidence in the correctness of the pixels that are correctly estimated as well.

3.3.1 Adaptive Depth Estimation

The advantages of these techniques can also be combined to minimize latency while maximizing the information about the scene. Consider the case of perception for autonomous navigation: selective depth can be used for the region directly in front of the ego vehicle, yielding high depth quality in the region that affects the most immediate decisions. However, information about farther objects cannot be completely dismissed. Rather than using additional sensors, such as radar, farther objects can be monitored with binary depth, which would act as a geo-fence that moves with the ego vehicle. This situation is depicted in Figure 7 at t_0, where top view indicates the selective range in green and the binary depth plane in blue. When the red van crosses the blue plane (t_1) the range of the selective depth can be extended to cover a larger region (t_2) yielding information about the van ap-
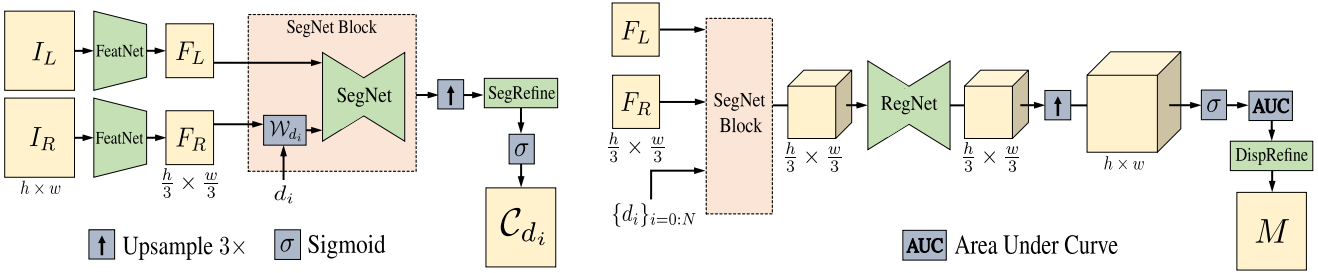
Figure 6: Bi3DNet, our core network, takes the stereo pair and a disparity d_i and produces a confidence map (Equation 4), which can be thresholded to yield the binary segmentation (left). To estimate depth on L quantization levels (Section 3.2) we run this network $L-1$ times and maximize the probability in Equation 8. To estimate continuous depth, whether full or selective, we run the SegNet block of Bi3DNet for each disparity level and work directly on the confidence volume (right).

proaching. This application is best show-cased with a video, which we provide in the supplementary video.

4. Implementation

In this section we provide high-level details for our implementation. More details are in the Supplementary.

The core of our method is a network that takes in a stereo pair and a disparity level d_i, and produces a binary segmentation with respect to π_{d_i}. We call this network Bi3DNet, see Figure 6 (left). The first module, FeatNet, which extracts features from the stereo images, is a simplified version of the feature extractor of PSMNet [1]. The output is a 32-channel feature map at a third of the resolution of the original image. FeatNet needs to run only once, regardless of the number of depth planes we seek to test. The left-image features and the warped right-image features are then fed to SegNet, a standard 2D encoder-encoder network with skip connections. Our SegNet architecture downsamples the input 5 times. At each scale in the encoder, we have a conv layer with stride of 2 followed by a conv layer with stride of 1. The decoder follows the same approach, where at each scale we have a deconv layer with a stride of 2 followed by a conv layer with a stride of 1. A final conv layer estimates the output of SegNet, which we bilinearly upsample to the original resolution. We then refine it with a light, 3-layer convolutional module (SegRefine), which also takes the input left image for guidance (not shown in Figure 6).

Estimating continuous or quantized depth, then, simply requires to run Bi3DNet multiple times. For quantized depth we use Bi3DNet directly, stack the $\mathcal{C}_{d_i}$'s, and maximize the probability in Equation 8. Note that, in order for the network to be agnostic to the number and the spacing of the disparity planes, we run the refinement module SegRefine independently for each disparity plane. For continuous depth, whether full or selective, the distance between the planes is fixed and known before-hand. Therefore, rather than applying a refinement to each binary segmentation, we

apply a 3D encoder-decoder module to the stacked outputs of the SegNet block, dubbed RegNet in Figure 6, (right). Using a single module on the volume, rather than multiple modules on each of the confidence maps, is more efficient and leads to better results since it can use information from the neighboring disparity planes. RegNet is closely inspired by the regularization module of GC-Net [11], with minor modifications described in the supplementary, also takes the left-image features as input for regularization. The final step is the refinement proposed in StereoNet [12], which takes the left image and the output of the AUC layer to generate the final disparity map, M.

Training. We first train Bi3DNet on the SceneFlow dataset. We form a batch with 64 stereo pairs and, for each of them, we randomly select a disparity plane for the segmentation. We use a binary cross-entropy (BCE) loss and train for 1k epochs. To train for continuous depth estimation, we initialize FeatNet and SegNet with the weights trained for binary depth. We form a batch with 8 stereo pairs and use two different losses: a BCE loss on the estimated segmentation confidence volume and SmoothL1 loss on the estimated disparity with weights of 0.1 and 0.9, respectively. We train this network for 100 epochs. For the KITTI dataset, we fine-tune both networks starting from the weights for SceneFlow. For both binary and continuous depth we use a batch size of 8 and the procedure described above, but we train them for 5k and 500 epochs, respectively. We use random crops of size 384x576, the Adam optimizer, and the maximum disparity of the planes we sample is 192 for all the trainings.

5. Evaluation and Results

Our goal is to offer a trade-off between latency and depth estimation accuracy—from binary depth, all the way to full continuous depth. While no existing method is designed to deal with quantized depth, we compare against two state-of-the-art (standard) stereo methods: GA-Net [28],
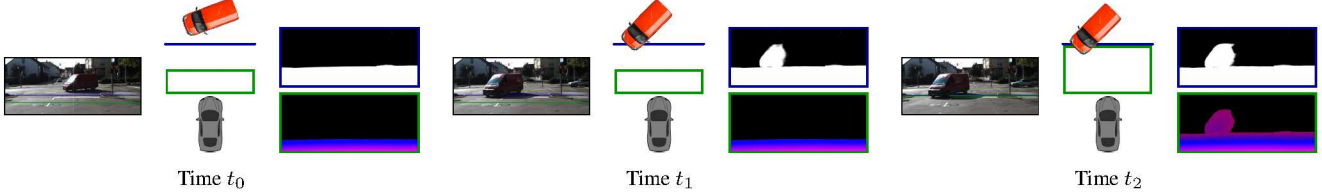
Figure 7: By combining selective and binary depth estimation, we can implement a simple adaptive depth estimation strategy, here shown for the automotive case. We can perform selective depth estimation for a close range (in green in the top view) to best use a given budget of disparity planes. We also monitor farther ranges with binary depth (blue plane). After an object crosses the far plane (t_1) the selective range can be adapted to yield accurate information about the distance (t_2).

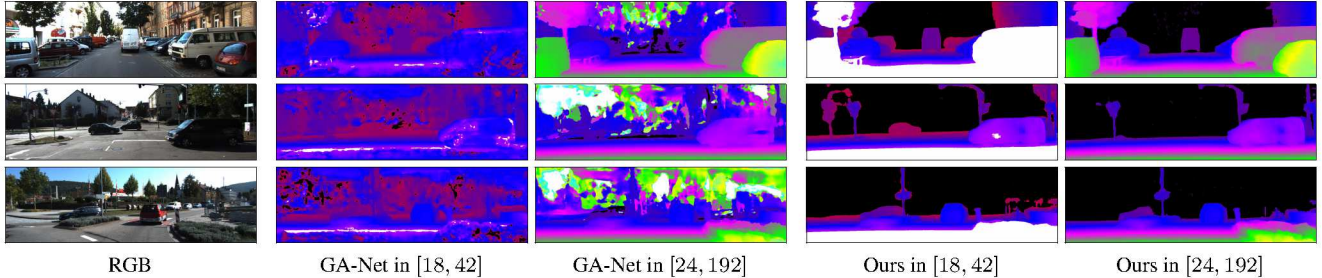| RGB | GA-Net in [18, 42] | GA-Net in [24, 192] | Ours in [18, 42] | Ours in [24, 192] |

Figure 8: Example of selective depth estimation for three different scenes and with two different disparity ranges, indicated in the labels. Our method predicts the correct depth in the range of interest. White and black pixels are those detected as being in front or behind the selected range.

top-performing method on KITTI at the time of submission, and DeepPruner [4], because the "fast" version is among the fastest high-performing methods on KITTI. Because these methods are not designed to estimate depth quantization directly, we run them to compute the full depth and then quantize it appropriately. Because quantized depth estimation is a segmentation problem, we evaluate the results with the mean intersection over union (mIOU) with the depth labels used as classes. Table 2 shows the results using 1k randomly selected images from the Scene Flow Dataset [17]. Notice that our method yields a higher mIOU despite having access to less information (fewer disparity planes). Perhaps more importantly, however, our method can run as fast as 5.3ms (> 180fps) for binary depth, or 9.8ms (> 100fps) with four levels of quantization (measured on a NVIDIA Tesla V100 with TensorRT). The runtime depends on the specific implementation and hardware, and thus a direct comparison is not entirely fair, however, for reference, DeepPrunerFast reports 62ms.[2] Figure 5 shows results of quantized depth for 4, 8, and 16 levels of quantization. Note that, 4 and 8 levels are often enough to form a rough idea of the scene.

We also compare our algorithm for full, continuous depth estimation against state-of-the-art methods. Tables 3 and 1 show results on KITTI 2015 and Scene Flow respectively. Although the strength and true motivation for our method is

its flexibility to the choice of the depth range, our numbers are surprisingly close to state-of-the-art methods that specifically target these benchmarks. On the Scene Flow dataset our EPE is the second best, Table 1.

Moreover, a visual comparison with recent GA-Net [28] and GwcNet [7] shows a comparable quality, see Figure 9.

6. Conclusions

In this paper we introduce a novel framework for stereo-based depth estimation. We show that we can learn to classify which regions of the scene are in front or beyond a virtual fronto-parallel plane. By performing many such tests and finding at which plane the classification of each pixel switches labels, we can can estimate accurate depth. More importantly, however, it allows to effectively focus on specific depth ranges. This can reduce the computational load or improve depth quality under a budget on the number of disparities that can be tested. Although our focus is on the ability to define a flexible depth range, we also show that our method close or on par with recent, highly-specialized methods.

Acknowledgments

---

[2]The authors of GA-Net provide the execution only time for their fast version (50-66ms for images of roughly half the size of ours), but not the corresponding trained model.

RGB   GwcNET [7]   GA-Net [28]   **Ours**
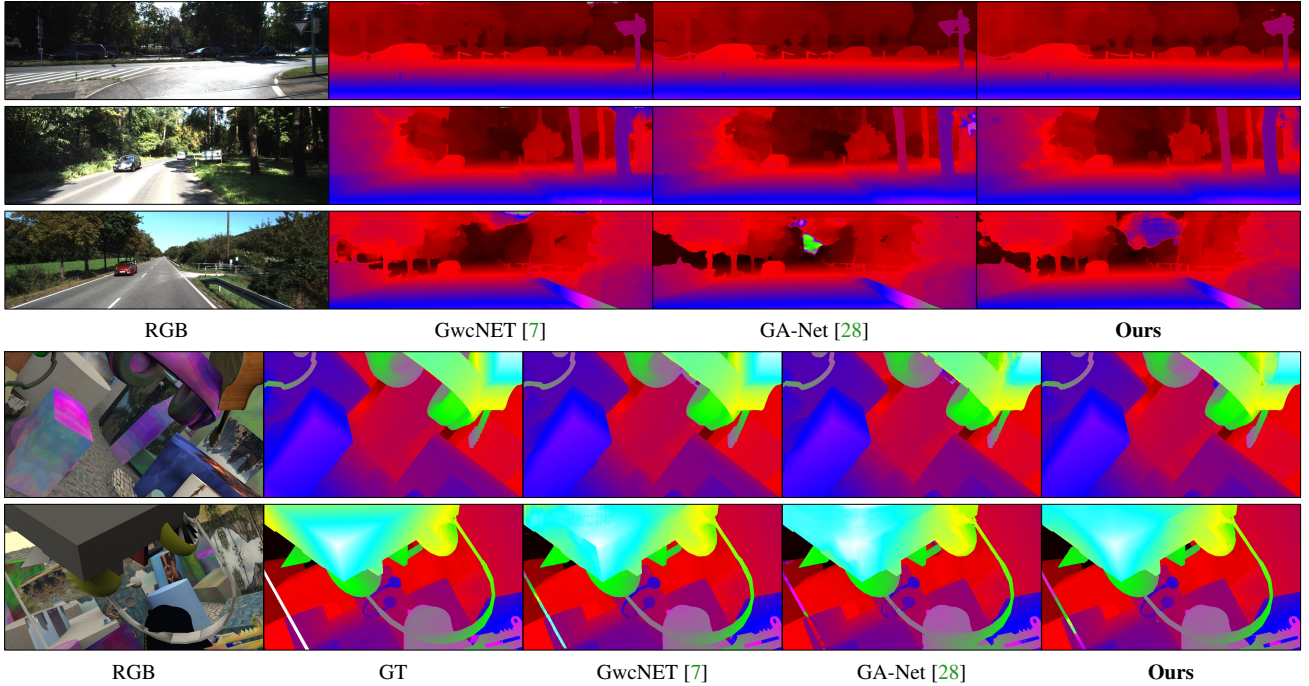
RGB   GT   GwcNET [7]   GA-Net [28]   **Ours**

Figure 9: Results for standard stereo for both KITTI and the Flying Things datasets. While our goal is an algorithm that allows flexible selection of the range, even on traditional stereo (*i.e.*, looking for correspondences across the whole range) our method produces results visually comparable to the state-of-the-art. In fact, in regions such as the power lines in the KITTI results, our results are visually better than those of GA-Net, the top-ranked method on the KITTI benchmark.

GC-Net [11]	DipsNetC [16]	CRL [19]	PDS-Net [24]	PSM-Net [1]	DeepPruner [4]	GANet-15 [28]	CSPN [2]	MCUA [18]	GwcNet [7]	**Ours**
2.51	1.68	1.32	1.12	1.09	0.86	0.84	0.78	0.56	0.76	**0.73**

Table 1: EPE values on the Scene Flow dataset for several state-of-the-art methods. Our method has the second best score.

		GA-Net	DeepPrunerFast	Ours (Time)
	2	0.9654	0.9677	0.9702 (5.3ms)
Levels	4	0.9302	0.9350	0.9372 (9.8ms)
	8	0.8774	0.8826	0.8909 (18.5ms)
	16	0.8061	0.8066	0.8307 (36ms)

Table 2: Mean IOU for different levels of depth quantization (higher is better). For GA-Net and DeepPruner we quantize the full depth, see text. Note that our method is on par in terms of quality, but offers the ability to trade depth accuracy for latency. For reference DeepPrunerFast, which is faster than GA-Net, runs in 62ms.

References

[1] Jia-Ren Chang and Yong-Sheng Chen. Pyramid stereo matching network. In *Proceedings of the IEEE Conference on Computer Vision and Pattern Recognition (CVPR)*, 2018. 3, 6, 8

[2] Xinjing Cheng, Peng Wang, and Ruigang Yang. Depth estimation via affinity learned with convolutional spatial propagation network. In *Proceedings of the European Conference on Computer Vision (ECCV)*, pages 103–119, 2018. 8

	Noc (%)			All (%)		
Methods	bg	fg	all	bg	fg	all
MAD-Net [23]	3.45	8.41	4.27	3.75	9.2	4.66
Content-CNN [15]	3.32	7.44	4.00	3.73	8.58	4.54
DipsNetC [16]	4.11	3.72	4.05	4.32	4.41	4.34
MC-CNN [27]	2.48	7.64	3.33	2.89	8.88	3.89
GC-Net [11]	2.02	3.12	2.45	2.21	6.16	2.87
CRL [19]	2.32	3.68	2.36	2.48	3.59	2.67
PDS-Net [24]	2.09	3.68	2.36	2.29	4.05	2.58
PSM-Net [1]	1.71	4.31	2.14	1.86	4.62	2.32
SegStereo [25]	1.76	3.70	2.08	1.88	4.07	2.25
AutoDispNet-CSS [20]	1.80	2.98	2.00	1.94	3.37	2.18
EdgeStereo [22]	1.72	3.41	2.00	1.87	3.61	2.16
DeepPruner-Best [4]	1.71	3.18	1.95	1.87	3.56	2.15
GwcNet [7]	1.61	3.49	1.92	1.74	3.93	2.11
EMCUA [18]	1.50	3.88	1.90	1.66	4.27	2.09
GANet-15 [28]	1.40	3.37	1.73	1.55	3.82	1.93
CSPN [2]	1.40	2.67	1.61	1.51	2.88	1.74
Ours	**1.79**	**3.11**	**2.01**	**1.95**	**3.48**	**2.21**

Table 3: Numerical results on the KITTI dataset. Our method outperforms several authoritative methods, such as PDS-Net [24] and GC-Net [11].

[3] Robert T Collins. A space-sweep approach to true multi-image matching. In *Proceedings of the IEEE Conference on Computer Vision and Pattern Recognition (CVPR)*, 1996. 3

[4] Shivam Duggal, Shenlong Wang, Wei-Chiu Ma, Rui Hu, and Raquel Urtasun. DeepPruner: Learning efficient stereo matching via differentiable patchmatch. In *Proceedings of the IEEE Conference on Computer Vision and Pattern Recognition (CVPR)*, 2019. 1, 3, 7, 8

[5] Andreas Geiger, Philip Lenz, Christoph Stiller, and Raquel Urtasun. Vision meets robotics: The kitti dataset. *The International Journal of Robotics Research*, 32(11):1231–1237, 2013. 3, 4

[6] Andreas Geiger, Martin Roser, and Raquel Urtasun. Efficient large-scale stereo matching. In *Proceedings of the Asian Conference on Computer Vision (ACCV)*, 2010. 2

[7] Xiaoyang Guo, Kai Yang, Wukui Yang, Xiaogang Wang, and Hongsheng Li. Group-wise correlation stereo network. In *Proceedings of the IEEE Conference on Computer Vision and Pattern Recognition (CVPR)*, June 2019. 4, 7, 8

[8] Heiko Hirschmuller. Accurate and efficient stereo processing by semi-global matching and mutual information. In *Proceedings of the IEEE Conference on Computer Vision and Pattern Recognition (CVPR)*, 2005. 2

[9] Heiko Hirschmuller and Daniel Scharstein. Evaluation of cost functions for stereo matching. In *Proceedings of the IEEE Conference on Computer Vision and Pattern Recognition (CVPR)*, 2007. 2

[10] Sunghoon Im, Hae-Gon Jeon, Stephen Lin, and In So Kweon. DPSNet: End-to-end deep plane sweep stereo. *arXiv preprint arXiv:1905.00538*, 2019. 3

[11] Alex Kendall, Hayk Martirosyan, Saumitro Dasgupta, Peter Henry, Ryan Kennedy, Abraham Bachrach, and Adam Bry. End-to-end learning of geometry and context for deep stereo regression. In *Proceedings of the IEEE Conference on Computer Vision and Pattern Recognition (CVPR)*, 2017. 3, 6, 8

[12] Sameh Khamis, Sean Fanello, Christoph Rhemann, Adarsh Kowdle, Julien Valentin, and Shahram Izadi. StereoNet: Guided hierarchical refinement for real-time edge-aware depth prediction. In *Proceedings of the European Conference on Computer Vision (ECCV)*, 2018. 1, 6

[13] Andreas Klaus, Mario Sormann, and Konrad Karner. Segment-based stereo matching using belief propagation and a self-adapting dissimilarity measure. In *IEEE International Conference on Pattern Recognition (ICPR'06)*, 2006. 2

[14] Vladimir Kolmogorov and Ramin Zabih. Computing visual correspondence with occlusions via graph cuts. 2001. 2

[15] W. Luo, A. G. Schwing, and R. Urtasun. Efficient deep learning for stereo matching. In *Proceedings of the IEEE Conference on Computer Vision and Pattern Recognition (CVPR)*, pages 5695–5703, June 2016. 8

[16] Nikolaus Mayer, Eddy Ilg, Philip Hausser, Philipp Fischer, Daniel Cremers, Alexey Dosovitskiy, and Thomas Brox. A large dataset to train convolutional networks for disparity, optical flow, and scene flow estimation. In *Proceedings of the IEEE Conference on Computer Vision and Pattern Recognition (CVPR)*, 2016. 3, 8

[17] Moritz Menze and Andreas Geiger. Object scene flow for autonomous vehicles. In *Proceedings of the IEEE Conference on Computer Vision and Pattern Recognition (CVPR)*, 2015. 7

[18] Guang-Yu Nie, Ming-Ming Cheng, Yun Liu, Zhengfa Liang, Deng-Ping Fan, Yue Liu, and Yongtian Wang. Multi-level context ultra-aggregation for stereo matching. In *Proceedings of the IEEE Conference on Computer Vision and Pattern Recognition (CVPR)*, pages 3283–3291, 2019. 8

[19] J. Pang, W. Sun, J. S. Ren, C. Yang, and Q. Yan. Cascade residual learning: A two-stage convolutional neural network for stereo matching. In *Proceedings of the IEEE International Conference on Computer Vision (ICCV)*, pages 878–886, Oct. 2017. 8

[20] Tonmoy Saikia, Yassine Marrakchi, Arber Zela, Frank Hutter, and Thomas Brox. AutoDispNet: Improving disparity estimation with automl. In *Proceedings of the IEEE International Conference on Computer Vision (ICCV)*, 2019. 8

[21] Daniel Scharstein and Richard Szeliski. A taxonomy and evaluation of dense two-frame stereo correspondence algorithms. *International Journal of Computer Vision (IJCV)*, 2002. 1, 2

[22] Xiao Song, Xu Zhao, Hanwen Hu, and Liangji Fang. EdgeStereo: A context integrated residual pyramid network for stereo matching. *arXiv*, 2018. 8

[23] Alessio Tonioni, Fabio Tosi, Matteo Poggi, Stefano Mattoccia, and Luigi Di Stefano. Real-time self-adaptive deep stereo. In *Proceedings of the IEEE Conference on Computer Vision and Pattern Recognition (CVPR)*, 2019. 8

[24] Stepan Tulyakov, Anton Ivanov, and François Fleuret. Practical deep stereo (PDS): Toward applications-friendly deep stereo matching. In *Advances in Neural Information Processing Systems (NIPS)*, 2018. 8

[25] Guorun Yang, Hengshuang Zhao, Jianping Shi, Zhidong Deng, and Jiaya Jia. SegStereo: Exploiting semantic information for disparity estimation. In *Proceedings of the European Conference on Computer Vision (ECCV)*, 2018. 8

[26] Ramin Zabih and John Woodfill. Non-parametric local transforms for computing visual correspondence. In *Proceedings of the European Conference on Computer Vision (ECCV)*, 1994. 2

[27] Jure Zbontar and Yann LeCun. Computing the stereo matching cost with a convolutional neural network. In *Proceedings of the IEEE Conference on Computer Vision and Pattern Recognition (CVPR)*, 2015. 3, 8

[28] Feihu Zhang, Victor Prisacariu, Ruigang Yang, and Philip HS Torr. GA-Net: Guided aggregation net for end-to-end stereo matching. In *Proceedings of the IEEE Conference on Computer Vision and Pattern Recognition (CVPR)*, 2019. 3, 4, 5, 6, 7, 8